Journal of Computational Applied Mechanics 2021, 52(3): 478-497
DOI: 10.22059/jcamech.2021.326538.636

RESEARCH PAPER

Forced vibration of a magnetoelastic laminated composite beam on Pasternak's foundation

Ashraf M. Zenkour[1,2*], Hela D. El-Shahrany[1,3]

[1] Department of Mathematics, Faculty of Science, King Abdulaziz University, P.O. Box 80203, Jeddah 21589, Saudi Arabia

[2] Department of Mathematics, Faculty of Science, Kafrelsheikh University, Kafrelsheikh 33516, Egypt

[3] Department of Mathematics, Faculty of Science, Bisha University, Bisha 61922, Saudi Arabia

Abstract

Vibrational behavior prediction of a laminated composite beam on Winkler-Pasternak's medium is analyzed in the present article. The proposed beam contains four smart actuating layers of magnetostrictive material to vibration control of the system with a simple constant feedback control gain distribution. The designed structure undergoes an external force in x direction and a magnetic field. A higher-order shear deformation theory with an exponential shape function is used to model the proposed system. Hamilton's principle and Navier's approach are used to obtain and solve the dynamic system. The natural frequencies, deflections, and suppression time of the studied system are computed for different thickness ratios, ply orientations, number and location of the magnetostrictive layers, foundation stiffness, velocity feedback gain value, and external force.

Keywords: Laminated composite beam, Magnetostrictive actuating layers, Higher-order shear deformation theory, Winkler-Pasternak's medium, External force.

Introduction

In engineering applications, smart structures are advanced multifunctional material systems that can appear some active influences and preserve the optimum environmental conditions. The adaptive structural systems having parts to perform functions such as control, actuation, and sensing. These functions can be performed by piezoelectric and magnetostrictive materials as smart materials. Vibration control strategies of systems can be obtained by these materials with broad frequency bandwidth, small packaging size, and high reliability. The magneto-mechanical coupling in the magnetostrictive material causes various unique behaviors which are relevant to the control of structural vibration such as the material hysteresis and the Joule, Villari, and Delta-E effects [1]. The magnetostriction phenomenon is the strong coupling between mechanical and magnetic properties of ferromagnetic materials, where, the applied magnetic field generates strain in the magnetostrictive material, conversely, the mechanical stress in this material produces measurable magnetization changes, therefore, This response can be employed for sensing and actuating functions [2]. The easy embeddability in the host materials without compromising the integrity of the structure and the remote excitation possibility are attractive advantages of the magnetostrictive materials to use for the active control of vibration as sensors and actuators, increasingly, in recent years. Especially,

* Corresponding Author. *Email Address*: zenkour@kau.edu.sa , zenkour@sci.kfs.edu.eg

embedding the magnetostrictive particles in the composite structural systems. Several theoretical studies have been focused on smart structures and laminated composite structures with/without magnetostrictive material layers.

Due to the low cost and a compromise between the lightness and stiffness, composite laminate applications are increasing in several fields of engineering applications such as aerospace, automotive and underwater. Therefore, their vibration behavior is a fundamental consideration for the composite structural system integrity. Many theories have been employed to analyze the dynamic characteristics of composite laminates. Classical theory neglects rotary inertia and shear deformation. This theory presents inaccurate natural frequency for composite laminates and the moderately or thick structure (e.g. [3]). First- and higher-order shear deformation theories [4] have been proposed to overcome the classical theory limitation. The first-order shear deformation theory assumes that a shear strain through the structure thickness is uniform, hence there is a need for a shear correction factor for the equilibrium. Whereas, higher-order shear deformation theories satisfy the zero shear stress condition at the structure surfaces and assume a realistic shear stress distribution through the structure thickness to overcome this limitation. Nejad et al. [5] conducted a review for some critical problems and issues to develop thick Functionally graded smart (piezoelectric) shells with focusing on simplified theories and mixed theories, elasticity theories, shear deformation theories in which were used to analyze these structures. Murty et al [6] discussed the influences of the lay-up sequence, the control gain, the weight of the coil and the concentrated mass on the dynamic motion and damping behavior of the flexible cantilever laminated composite beam contains Terfenol-D particle layer. Kumar et al. developed a finite element formulation to investigate the vibration reduction in an aluminum beam with a magnetostrictive layer for different boundary conditions [7], followed by studying the damping behavior of a titanium shell containing a magnetostrictive ply [8]. Lee et al. [9] presented a study to discuss the vibration damping characteristics of a laminated composite plate with smart (Terfenol D material) plies using the finite element method. Pradhan [10] investigated the influence of the material properties, the magnetostrictive layer location, and control parameters on the solution behavior of simply supported functionally graded material shells containing magnetostrictive plies. Zabihollah and Zareie [11] analyzed the smart laminated beam based on a layerwise theory using the finite element model, and they determined the optimal location/size of actuators/sensors for vibration control applications and dynamic displacement measurement purposes. Under mechanical and electrical loadings, Reddy [12] presented theoretical formulations, finite element models, and the Navier solutions to study the laminated composite plates with integrated actuators and sensors according to the classical and shear deformation theories. Santapuri et al. [13] presented a two-dimensional nonlinear model to describe the dynamic response of a Galfenol–aluminum composite actuator. Krishnamurthy et al. [14] presented an exploratory study to detect the delamination in polymeric laminated composite beam containing a Terfenol-D particles layer. Hong [15] presented a new technology application of a magnetostrictive actuator that can be used to the pollution reduction of mechanical parts in the green energy field where this application was constructed by thin laminate strip, support, and magnet to provide a good stroke length. Moon et al. [16] confirmed the Terfenol-D actuator's capability to control an aluminum beam by using a quadratic feedback controller. Kishore et al.[17] presented a geometric nonlinear analysis of a laminated composite plate with Terfenol-D layers according to a third-order shear deformation theory. Furthermore, many theoretical studies have been focused on the nonlinear behavior of structural systems containing magnetostrictive actuators for example [18-23]. Saidha et al. [24] presented an experimental study to demonstrate the efficacy of magnetostrictive patches for delamination detection in a smart laminated composite beam. Recently, Zhang et al. [25] combined the feedforward gain and feedback gain for achieving a good control influence in the structural

system containing the giant magnetostrictive actuator under the operating conditions of the sinusoidal and initial excitation. Shahin and Asghar [26] used the first-order shear deformation theory and the Ritz and modified Galerkin methods to analyze the vibration of an isotropic truncated conical shell with magnetostrictive actuators. Zenkour and El-Shahrany computed the natural frequencies of laminated composite beam with four Terfenol-D actuators according to a hyperbolic shear deformation theory in [27], followed by analyzing a linear model for dynamic response of the smart composite beam rested on a viscoelastic medium in [28]. Also, Zenkour and El-Shahrany [29] computed the natural frequencies and deflection of a laminated magnetostrictive composite sandwich plate with a homogenous core supported by a three-parameter foundation. Zarezadeh et al. [30] used the generalized differential quadrature method to solve the equations of functionally graded (FG) nano-rod supporting by a torsional foundation and under magnetic field. Barati et al. [31] analyzed static torsion of a bi-directional functionally graded microtube subjected on an axial magnetic field. Barati et al. [32] used a longitudinal magnetic field to control the vibrations of bi-directional functionally graded nanobeam. Under magnetic force and mechanical loads, Mousavi et al. [33] investigated the bending of bidirectional functionally graded nanobeam supported by the Pasternak's foundation.

In the present work, to effectively and accurately prediction of the natural vibrational behavior of the laminated composite beam with four magnetostrictive actuators rested on a two-parameter medium, the proposed structural model can be analyzed by taking into account the shear deformation impact and the in-plane force in x-direction influence where there is no study in the literature to discuss this effect on the vibrational behavior of the smart laminated beams. The uniform excitation presence can be assumed to achieve the forced motion under a constant distribution of the feedback gain control in the studied model. The forced vibration analysis of the proposed model is carried out based on a higher-order shear theory with exponential function to describe the stresses distribution through the thickness.

Mathematical model

A schematic figure (Figure 1) shows a laminated sandwich beam with length L. In general, the beam composes $k-4$ fiber-reinforced material plies along with four smart plies of magnetostrictive material in [(m)th, $(k-m+1)$th] and faces of the beam. The simply supported beam is subjected to in-plane force in the x-direction. According to an exponential higher-order deformation theory, the displacement field can be defined as

$$\begin{aligned} u(x,y,z,t) &= -z\frac{\partial w_0}{\partial x} + f(z)\varphi(x,t), \\ v(x,y,z,t) &= 0, \end{aligned} \tag{1}$$

$$w(x,y,z,t) = w_0(x,t),\ f(z) = z\mathrm{e}^{-2\left(\frac{z}{h}\right)^2}.$$

The two unknown functions w_0 and φ represent the transverse deflection and the rotation about y-axis. The simply supported beam rests on a two-parameter elastic foundation which can be described by the next equation.

$$E_f = K_W w_0 - K_P \frac{\partial^2 w_0}{\partial x^2}, \tag{2}$$

where K_P and K_W are the shear foundation (Pasternak's) parameter, and Winkler's spring modulus, respectively.

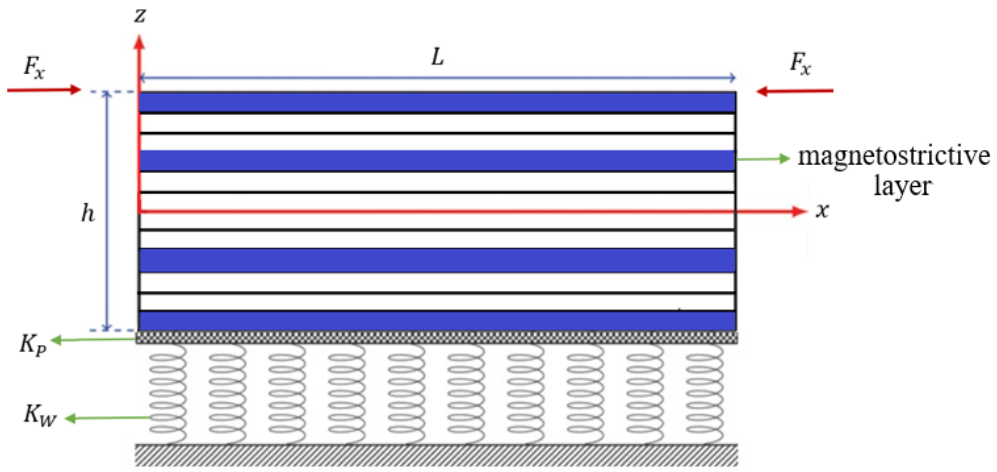

Figure 1. Schematic diagram of the beam.

Utilizing the relations of displacement–strain, the kinematic equations for smart beam according to exponential shear deformation theory can be obtained as

$$\varepsilon_{xx} = z\varepsilon_{xx}^{(1)} + f(z)\varepsilon_{xx}^{f}, \quad \gamma_{xz} = h(z)\gamma_{xz}^{h}, \tag{3}$$

where

$$\varepsilon_{xx}^{(1)} = -\frac{\partial^2 w_0}{\partial x^2}, \quad \varepsilon_{xx}^{f} = \frac{\partial \varphi}{\partial x}, \quad \gamma_{xz}^{h} = \varphi, \quad h(z) = f'(z). \tag{4}$$

1. Velocity feedback control and constitutive equations

The constitutive relation for the rth fiber-reinforced layer can be expressed as

$$\sigma_{xx}^{(r)} = \bar{Q}_{11}^{(r)}\varepsilon_{xx} - \bar{e}_{31}^{(m)}H, \qquad \bar{\gamma}_{xz} = \bar{Q}_{55}^{(r)}\gamma_{xz}, \tag{5}$$

where the transformed engineering constants $\bar{Q}_{ij}^{(r)}$ are given in Murty et al. [6] and $\bar{e}_{31}^{(m)}$ is the transformed magnetostrictive coupling moduli. The magnetic field intensity H relates to the coil current I by the following relationship

$$H(x,t) = k_c I(x,t), \;\; I(x,t) = c(t)\frac{\partial w_0}{\partial t}, \tag{6}$$

where $c(t)$ and k_c are the control gain and the coil constant.

Governing system

Equations of the motion are obtained via the following Hamilton's principle

$$\delta \int_0^t (U + V - K)\,\mathrm{d}t = 0, \tag{7}$$

where the δ operator means the variation operator. The coefficients K, V, and U are the kinetic energy, the potential of the external work done by loads and the strain energy can be determined as

$$0=\int_0^T\int_0^L\int_{-\frac{h}{2}}^{\frac{h}{2}}\left[\sigma_{xx}\left(z\delta\varepsilon_{xx}^{(1)}+f(z)\delta\varepsilon_{xx}^{f}\right)+\sigma_{xz}h(z)\delta\gamma_{xz}^{h}\right]\mathrm{d}A\mathrm{d}x\mathrm{d}t$$

$$-\int_0^T\int_0^L\int_A\rho\left[\left(-z\frac{\partial\dot{w}_0}{\partial x}+f(z)\dot{\varphi}\right)\left(-z\frac{\partial\delta\dot{w}_0}{\partial x}+f(z)\delta\dot{\varphi}\right)+\dot{w}_0\delta\dot{w}_0\right]\mathrm{d}A\mathrm{d}x\mathrm{d}t$$

$$+\int_0^T\int_0^L(E_f+F_x\frac{\partial^2w_0}{\partial x^2})\delta w_0\mathrm{d}x\mathrm{d}t,$$

or

$$0=\int_0^T\int_0^L\left\{\left(M_{xx}\delta\varepsilon_{xx}^{(1)}+S_{xx}\delta\varepsilon_{xx}^{f}\right)+Q_f\delta\gamma_{xz}^{h}+(E_f+F_x\frac{\partial^2w_0}{\partial x^2})\delta w_0\right.$$

$$\left.-\left[\left(I_2\frac{\partial\dot{w}_0}{\partial x}-I_f\dot{\varphi}\right)\frac{\partial\delta\dot{w}_0}{\partial x}+\left(-I_f\frac{\partial\dot{w}_0}{\partial x}+I_{ff}\dot{\varphi}\right)\delta\dot{\varphi}+I_0\dot{w}_0\delta\dot{w}_0\right]\right\}\mathrm{d}x\mathrm{d}t,$$

in the final formulation

$$0=\int_0^T\int_0^L\left\{\left(-\frac{\partial^2M_{xx}}{\partial x^2}+E_f+F_x\frac{\partial^2w_0}{\partial x^2}-I_2\frac{\partial^2\ddot{w}_0}{\partial x^2}+I_f\frac{\partial\ddot{\varphi}}{\partial x}+I_0\ddot{w}_0\right)\delta w_0\right.$$

$$\left.+\left(Q_f-\frac{\partial S_{xx}}{\partial x}-I_f\frac{\partial\ddot{w}_0}{\partial x}+I_{ff}\ddot{\varphi}\right)\delta\varphi\right\}\mathrm{d}x\mathrm{d}t$$

$$+\int_0^T\left\{-M_{xx}\frac{\partial\delta\dot{w}_0}{\partial x}+\left[\frac{\partial M_{xx}}{\partial x}+I_2\frac{\partial\ddot{w}_0}{\partial x}-I_f\ddot{\varphi}\right]\delta w_0+S_{xx}\,\delta\varphi\right\}_0^L\mathrm{d}t,$$

in which

$$\begin{Bmatrix}M_{xx}\\S_{xx}\end{Bmatrix}=\int_A\sigma_{xx}\begin{Bmatrix}z\\f(z)\end{Bmatrix}\mathrm{d}z=\begin{bmatrix}D_{11}&E_{11}\\E_{11}&E_{11}^{f}\end{bmatrix}\begin{Bmatrix}\varepsilon^{(1)}\\\varepsilon^{f}\end{Bmatrix}-\begin{Bmatrix}M_{xx}^{m}\\S_{xx}^{m}\end{Bmatrix},$$

$$Q_f=\int_A\sigma_{xz}\,h(z)\mathrm{d}z=E_{55}\gamma_{xz}^{h}, \tag{8}$$

where

$$\begin{Bmatrix}M_{xx}^{m}\\S_{xx}^{m}\end{Bmatrix}=k_cc(t)\sum_r\int_{z_r}^{z_{r+1}}\bar{e}_{31}\begin{Bmatrix}z\\f(z)\end{Bmatrix}H_z\,\mathrm{d}z=\begin{Bmatrix}\beta\\\gamma\end{Bmatrix}\frac{\partial w_0}{\partial t},$$

$$r=1,m,k-m+1,k,$$

$$\{D_{11},E_{11},E_{11}^{f}\}=\int_{-\frac{h}{2}}^{\frac{h}{2}}\bar{Q}_{11}^{(r)}\{z^2,zf(z),[f(z)]^2\}\mathrm{d}z,\quad E_{55}=\int_{-\frac{h}{2}}^{\frac{h}{2}}\bar{Q}_{55}^{(r)}[h(z)]^2\mathrm{d}z,$$

$$\{I_0,I_2,I_f,I_{ff}\}=\int_{-\frac{h}{2}}^{\frac{h}{2}}\rho\{1,z^2,zf(z),[f(z)]^2\}\mathrm{d}z. \tag{9}$$

where F_x is the uniform in-plane force that is applied on the plate in x direction. The coefficients M_{xx}, S_{xx} and Q_f are the stress resultants and I_0, I_2, I_f and I_{ff} are the mass inertias. Now, the governing dynamic system can be presented as

$$-\frac{\partial^2 M_{xx}}{\partial x^2}+E_f+F_x\frac{\partial^2 w_0}{\partial x^2}-I_2\frac{\partial^2 \ddot{w}_0}{\partial x^2}+I_f\frac{\partial \ddot{\varphi}}{\partial x}+I_0\ddot{w}_0=0, \tag{10}$$

$$-\frac{\partial S_{xx}}{\partial x}+Q_f-I_f\frac{\partial \ddot{w}_0}{\partial x}+I_{ff}\ddot{\varphi}=0. \tag{11}$$

The governing system in terms of the displacement field of exponential shear deformation theory becomes

$$D_{11}\frac{\partial^4 w_0}{\partial x^4}-E_{11}\frac{\partial^3 \varphi}{\partial x^3}+\beta\frac{\partial^3 w_0}{\partial x^2\partial t}+E_f+F_x\frac{\partial^2 w_0}{\partial x^2}-I_2\frac{\partial^2 \ddot{w}_0}{\partial x^2}+I_f\frac{\partial \ddot{\varphi}}{\partial x}+I_0\ddot{w}_0=0, \tag{12}$$

$$E_{11}\frac{\partial^3 w_0}{\partial x^3}-E_{11}^f\frac{\partial^2 \varphi}{\partial x^2}+\gamma\frac{\partial^2 w_0}{\partial x\partial t}+E_{55}\varphi-I_f\frac{\partial \ddot{w}_0}{\partial x}+I_{ff}\ddot{\varphi}=0. \tag{13}$$

Analytical solution

The next boundary conditions for simply supported edges are used to obtain the analytical solution of the vibration problem based on Navier's method

$$w=\varphi=M_{xx}=S_{xx}=0 \text{ at } x=0,L, \tag{14}$$

The following forms of solution can be used

$$\begin{aligned} w_0(x,t)&=\sum_{n=1}^{\infty}W_0\mathrm{e}^{(-\alpha_n\pm i\omega_n)t}\sin\frac{n\pi x}{L},\\ \varphi(x,t)&=\sum_{n=1}^{\infty}X_0\mathrm{e}^{(-\alpha_n\pm i\omega_n)t}\cos\frac{n\pi x}{L},\quad i=\sqrt{-1}, \end{aligned} \tag{15}$$

where W_0 and X_0 are arbitrary coefficients can be determined using the following initial conditions in Eq. (20). The parameter α_n is the damping coefficient and ω_n is the frequency for n mode number. By using the above solution form in Eq. (12) and Eq. (13), the dynamic equations become

$$\begin{bmatrix}\bar{S}_{11} & \bar{S}_{12}\\ \bar{S}_{21} & \bar{S}_{22}\end{bmatrix}\begin{Bmatrix}W_0\\ X_0\end{Bmatrix}=\begin{Bmatrix}0\\0\end{Bmatrix}. \tag{16}$$

The solution of the system in Eq.(16) can be determined as

$$\begin{vmatrix}\bar{S}_{11} & \bar{S}_{12}\\ \bar{S}_{21} & \bar{S}_{22}\end{vmatrix}=0, \tag{17}$$

in which

$$\bar{S}_{ij}=\hat{S}_{ij}+\lambda\widehat{M}_{ij}+\lambda^2\hat{C}_{ij},\quad i,j=1,2, \tag{18}$$

where the terms $\hat{S}_{ij}$, $\widehat{M}_{ij}$ and $\hat{C}_{ij}$ can be presented as

$$\hat{S}_{11}=D_{11}\left(\frac{n\pi}{L}\right)^4+(K_P+F_x)\left(\frac{n\pi}{a}\right)^2+K_W,\quad \hat{S}_{12}=\hat{S}_{21}=-E_{11}\left(\frac{n\pi}{L}\right)^3,\quad \hat{S}_{22}=E_{11}^f\left(\frac{n\pi}{L}\right)^2+E_{55},$$

$$\widehat{M}_{11}=-\beta\left(\frac{n\pi}{L}\right)^2,\quad \widehat{M}_{21}=\gamma\frac{n\pi}{L},\quad \widehat{M}_{12}=\widehat{M}_{22}=0,$$

$$\hat{C}_{11} = I_2\left(\frac{n\pi}{L}\right)^2 + I_0, \quad \hat{C}_{12} = -I_f\frac{n\pi}{L}, \quad \hat{C}_{22} = I_{ff},$$

The damping ratio ζ_n of mode n is defined as

$$\zeta_n = \frac{-\alpha_n}{\sqrt{{\alpha_n}^2 + {\omega_n}^2}}. \tag{19}$$

The next initial conditions can be applied to determine a particular solution

$$w(x,0) = 0, \qquad \dot{w}(x,0) = 1, \qquad \varphi(x,0) = 0, \qquad \dot{\varphi}(x,0) = 0. \tag{20}$$

The deflection of the smart beam can be presented as

$$w(x,t) = \frac{1}{\omega_n}\mathrm{e}^{-\alpha_n t}\sin\omega_n t\sin\frac{n\pi x}{L}. \tag{21}$$

The actuation stress can be presented as

$$\sigma_1(x,t) = -k_c c(t)\bar{e}_{31}^{(m)}\frac{\partial w_0}{\partial t}. \tag{22}$$

Numerical results and discussion

The vibration of the composite laminate with different lay-ups has been analyzed. The beam has four magnetostrictive actuators of the same thickness and supports by a two-parameter elastic medium. The beam undergoes multi-physical loads: an in-plane force in x direction and a uniform magnetic field generated by a coil in the transverse direction. Effects of the in-plane stresses are considered. The fiber-reinforced plies and smart layers are made of CFRP and Terfenol-D materials, respectively, where the properties of these materials have been presented in Reddy and Barbosa [30]. Moreover, the next geometric properties of the beam are used: $h/a = 0.06$, $K_W = K_P = 10^6$, $F_x = 10^3$, $k_c c(t) = 10^4$. The used ply-stacking sequence is $[m/\pm 45/0/90/m]_s$ to plot the numerical results of the proposed composite laminate dynamic response and the $[m/m/\pm 45/0/90]_s$ ply-stacking sequence to plot the deflection response of the proposed composite laminate. The in-plane force and foundation elements can be ignored in the current model to discuss the validation of the present study results that obtained based on exponential shear deformation theory (EXDT) by comparing with those results in Zenkour and El-Shahrany [27] which given according to Hyperbolic shear deformation theory (HSDT). It is noticeable that there is a great agreement between the results of the two theories as displayed in Table 1.

Table 1. Suppression time for various locations of magnetostrictive layers in laminates with $c(t)k_c = 10^4$, $h/a = 0.012$.

Lamination	Theory	$-\alpha_1 \pm \omega_1$	$W_{\max}$	$t(\mathrm{s})$	ζ_n
$[m/\pm 45/0/90/m]_s$[27]	HSDT	5.08±108.06	9.254	0.453	0.047
$[m/\pm 45/0/90/m]_s$	EXDT	5.079±108.065	9.254	0.453	0.0469
$[m/\pm 45/0/m/90]_s$[27]	HSDT	5.93±108.45	9.221	0.389	0.055
$[m/\pm 45/0/m/90]_s$	EXDT	5.925±108.447	9.221	0.389	0.055
$[m/\pm 45/m/0/90]_s$[27]	HSDT	6.77±100.24	9.976	0.340	0.067
$[m/\pm 45/m/0/90]_s$	EXDT	6.772±100.244	9.976	0.340	0.067
$[m/45/m/-45/0/90]_s$[27]	HSDT	7.62±98.41	10.162	0.302	0.077

$[m/45/m/-45/0/90]_s$	EXDT	7.618±98.404	10.162	0.302	0.077
$[m/m/\pm45/0/90]_s$[27]	HSDT	8.46±95.91	10.426	0.272	0.088
$[m/m/\pm45/0/90]_s$	EXDT	8.464 ±95.912	10.426	0.272	0.088

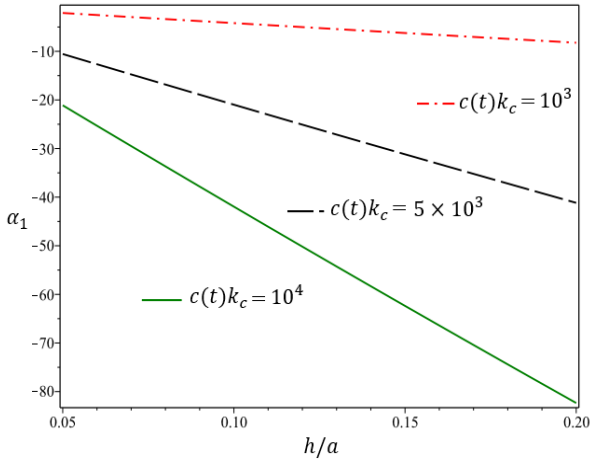

Figure 2. The first damping coefficient variation with the thickness ratio change for different values of the feedback gain control constant.

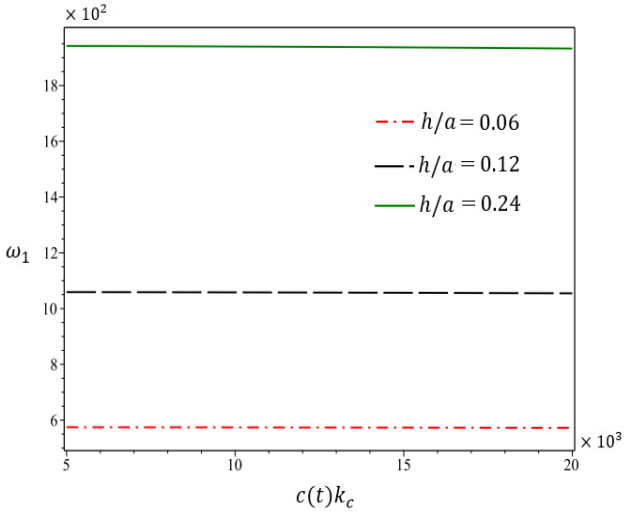

Figure 3. The first linear frequency variation with the feedback gain control change for different values of the thickness ratio.

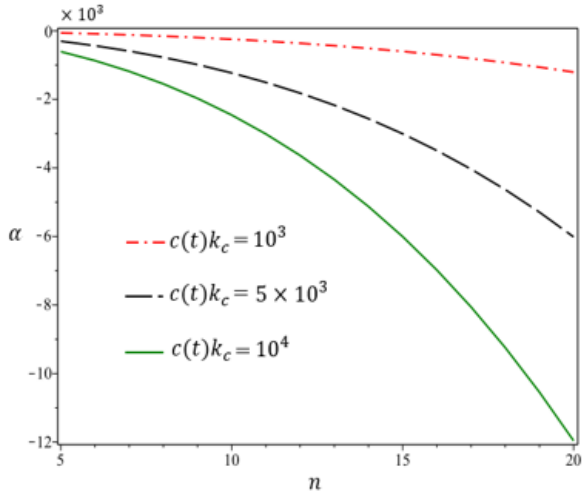

Figure 4. The damping coefficient variation with the half wave number change for different values of the feedback gain control constant.

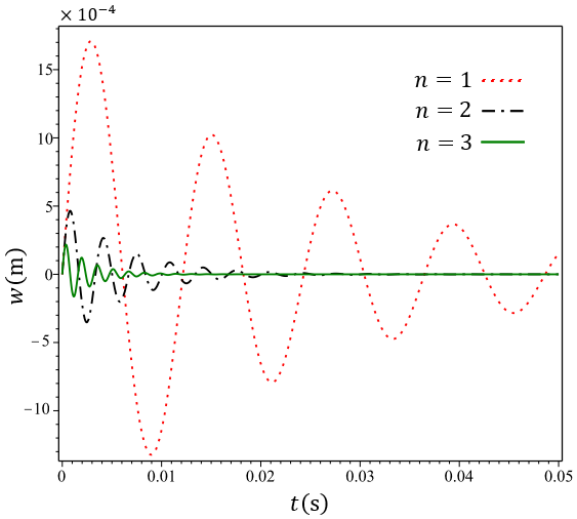

Figure 5. The deflection response of the studied beam with the damping time variation for different mode numbers.

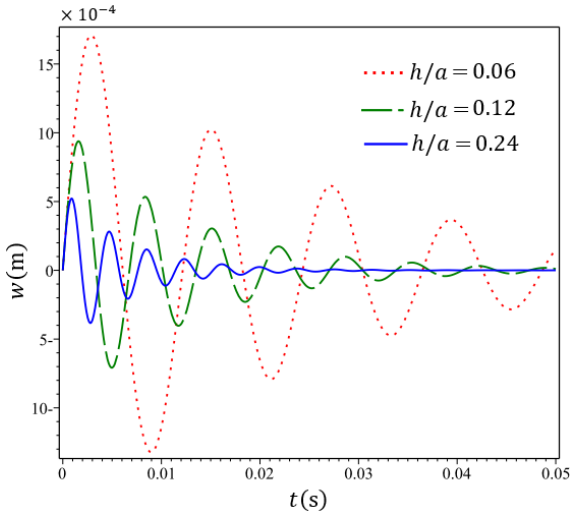

Figure 6. The deflection of the studied beam with the damping time change for different thickness ratios.

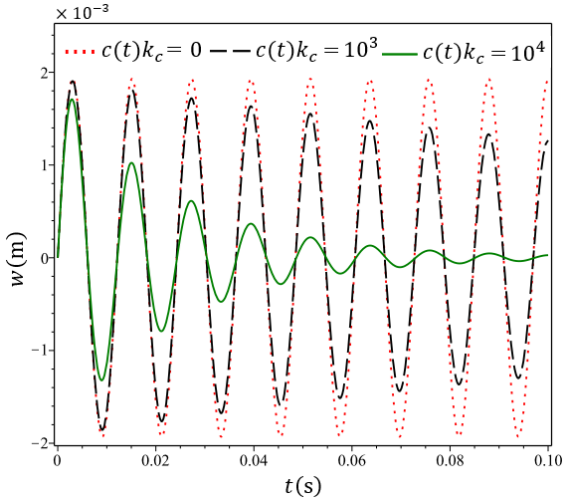

Figure 7. The deflection of the studied beam with the damping time change for different values of the feedback gain control.

Table 2. Eigenfrequency coefficients $-\alpha_n \pm \omega_n$ (rad s^{-1}) for different values of the thickness ratio, feedback gain control, and half wave number.

Laminate	h/a	$c(t)k_c$	n		
			1	2	3
$[m/\pm45/0/90/m]_s$	0.06	10^3	2.531±574.583	10.036±2135.685	22.322±4597.959
		5×10^3	12.657±574.449	50.182±2135.119	111.609±4596.659
		10^4	25.314±574.030	100.364±2133.349	223.219±4592.594
	0.12	10^3	5.018±1059.417	19.617±3889.526	43.508±7882.189
		5×10^3	25.091±1059.132	98.086±3888.340	217.541±7879.326
		10^4	50.182±1058.240	196.173±3884.632	435.090±7870.370
	0.24	10^3	9.809±1942.510	38.717±6264.200	90.896±11342.610
		5×10^3	49.043±1941.916	193.587±6261.366	454.480±11333.859
		10^4	98.086±1940.060	387.189±6252.499	908.956±11306.470
$[m/\pm45/m/0/90]_s$	0.06	10^3	3.374±538.469	13.364±1980.519	29.692±4238.480
		5×10^3	16.869±538.215	66.819±1979.437	148.459±4235.984
		10^4	33.378±537.422	133.637±1976.051	296.917±4228.176
	0.12	10^3	6.682±981.181	26.074±3563.383	57.764±7144.269
		5×10^3	33.409±980.635	130.369±3561.096	288.822±7138.706
		10^4	66.819±978.926	260.740±3553.942	577.666±7121.291
	0.24	10^3	13.037±1779.240	51.284±5623.801	118.565±10033.025
		5×10^3	65.185±1778.095	256.431±5618.273	592.851±10016.386
		10^4	130.370±1774.513	512.915±5600.958	1185.864±9964.185
$[m/m/\pm45/0/90]_s$	0.06	10^3	4.213±518.285	16.653±1885.226	36.921±3994.209
		5×10^3	21.067±517.874	83.266±1883.460	184.607±3990.114
		10^4	42.133±516.587	166.532±1877.931	369.216±3977.291
	0.12	10^3	8.327±933.100	32.380±3321.051	71.732±6520.337
		5×10^3	41.633±932.208	161.902±3317.270	358.672±6510.960
		10^4	83.266±929.415	323.810±3305.426	717.416±6481.559
	0.24	10^3	16.190±1657.912	63.767±5034.766	147.377±8686.378
		5×10^3	80.951±1656.018	318.862±5025.252	736.987±8656.831
		10^4	161.906±1650.087	637.885±4995.382	1474.598±8563.699

Variation of the closed-loop frequencies and damping coefficients concerning the changes in the thickness ratio, controller gain, and half wave number is displayed in Table 2 for three different positions of the active inner layers. It can be observed that the damping coefficients and the closed-loop frequencies increase with the rising values of the thickness ratio and mode number. But the damping coefficient increases obviously and the frequency insignificantly decreases with increasing the feedback gain control value. This effect can be displayed in Figures 2 and 3 where it can be seen that increase of the feedback gain control value leads to the damping coefficients $|\alpha|$ increase significantly and the frequencies very slightly (constant almost) reduce whereas all of the eigenfrequency coefficients increase highly by increasing the thickness ratio. For different values of the feedback gain control parameter, Figure 4 depicts the damping coefficient variation with the half wave number change. It can be observed that by increasing the mode numbers and/or the feedback gain control values, the vibration damping process improves. The deflection response of the studied system with the damping time variation for some factors: mode numbers, thickness ratio, and the feedback gain control is shown in Figures 5-7, respectively. It is noted that a decrement in the deflections because the damping coefficients increase due to rising values of these parameters. Figure 7 includes also the uncontrolled motion of the presented model in absence of the controller gain. Uncontrolled time and uncontrolled large amplitude

of the deflection for the smart beam are observed in this case. So, the controller gain plays important role in vibration control of the system.

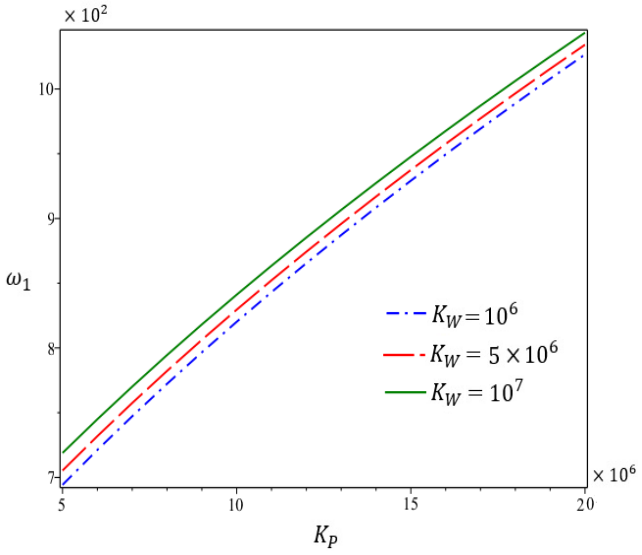

Figure 8. The first linear frequency variation with the shear layer stiffness change for different values of the Winkler's spring modulus.

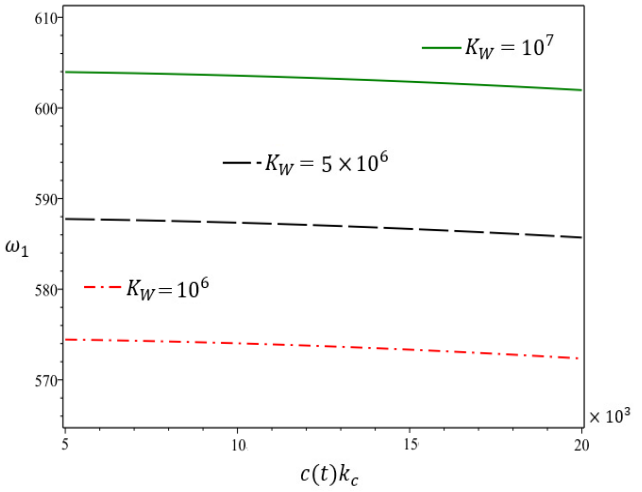

Figure 9. The first linear frequency variation with the feedback gain control change for different values of the Winkler's spring modulus.

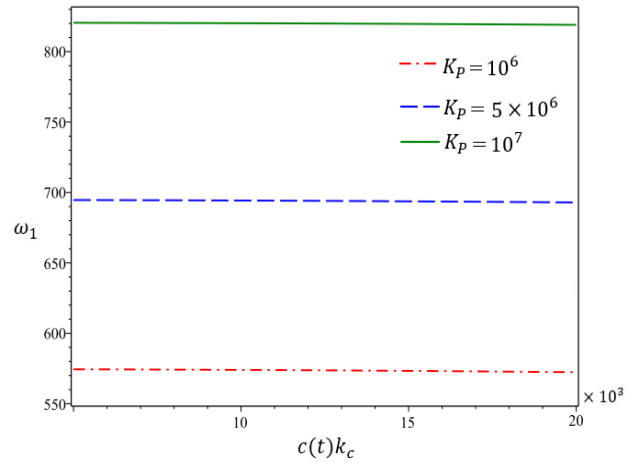

Figure 10. The first linear frequency variation with the feedback gain control change for different values of the shear layer stiffness constant.

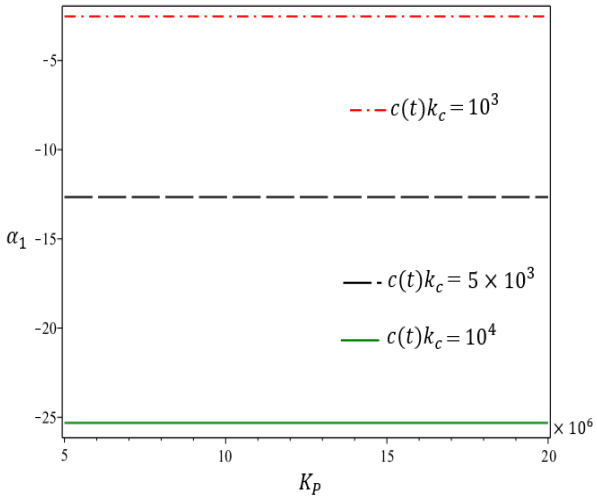

Figure 11. The first damping coefficient variation with the shear layer stiffness change for different values of the feedback gain control constant.

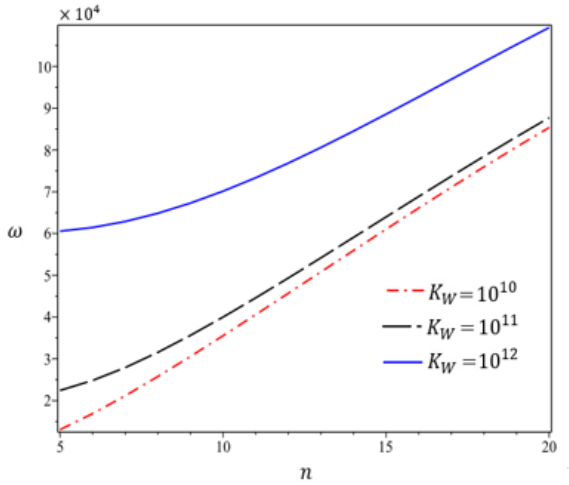

Figure 12. The linear frequency variation with the half wave number change for different values of the Winkler's spring modulus.

Table 3. Eigenfrequency coefficients $-\alpha_1 \pm \omega_1$ (rad s^{-1}) for different values of the foundation constant and the external force.

Laminate	K_W	F_x	K_P		
			0	10^6	5×10^6
$[m/\pm 45/0/90/m]_s$	10^6	0	25.314±539.830	25.314±574.064	25.314±694.321
		10^3	25.314±539.794	25.314±574.030	25.314±694.293
		-10^3	25.314±539.865	25.314±574.097	25.314±694.348
		10^6	25.314±503.272	25.314±539.830	25.314±666.294
		-10^6	25.314±574.064	25.314±606.368	25.314±721.259
	5×10^6	0	25.314±553.959	25.314±587.370	25.314±705.362
		10^3	25.314±553.925	25.314±587.338	25.314±705.335
		-10^3	25.314±553.994	25.314±587.403	25.314±705.389
		10^6	25.314±518.399	25.314±553.959	25.314±677.793
		-10^6	25.314±587.370	25.314±618.980	25.314±618.980

	10^7	0	25.314±571.130	25.314±603.591	25.314±718.926
		10^3	25.314±571.096	25.314±603.560	25.314±718.899
		-10^3	25.314±571.163	25.314±603.623	25.314±718.952
		10^6	25.314±536.709	25.314±571.130	25.314±691.897
		-10^6	25.314±603.591	25.314±634.394	25.314±744.975
$[m/m/\pm45/0/90]_s$	10^6	0	42.133±478.349	42.133±516.623	42.133±647.479
		10^3	42.133±478.309	42.133±516.587	42.133±647.449
		-10^3	42.133±478.388	42.133±516.660	42.133±647.508
		10^6	42.133±436.732	42.133±478.349	42.133±617.371
		-10^6	42.133±516.623	42.133±552.252	42.133±676.248
	5×10^6	0	42.133±494.218	42.133±531.351	42.133±659.290
		10^3	42.133±494.180	42.133±531.315	42.133±659.261
		-10^3	42.133±494.257	42.133±531.387	42.133±659.319
		10^6	42.133±454.059	42.133±494.218	42.133±629.747
		-10^6	42.133±531.351	42.133±566.053	42.133±687.565
	10^7	0	42.133±513.366	42.133±549.205	42.133±673.762
		10^3	42.133±513.329	42.133±549.171	42.133±673.734
		-10^3	42.133±513.403	42.133±549.240	42.133±673.791
		10^6	42.133±474.828	42.133±513.366	42.133±644.883
		-10^6	42.133±549.205	42.133±582.846	42.133±701.454

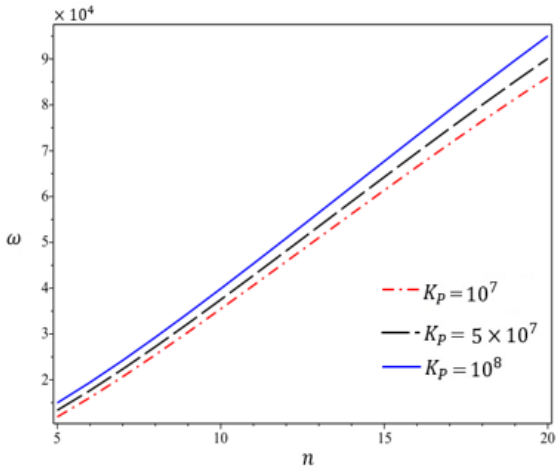

Figure 13. The linear frequency variation with the mode number change for different values of the shear layer stiffness constant.

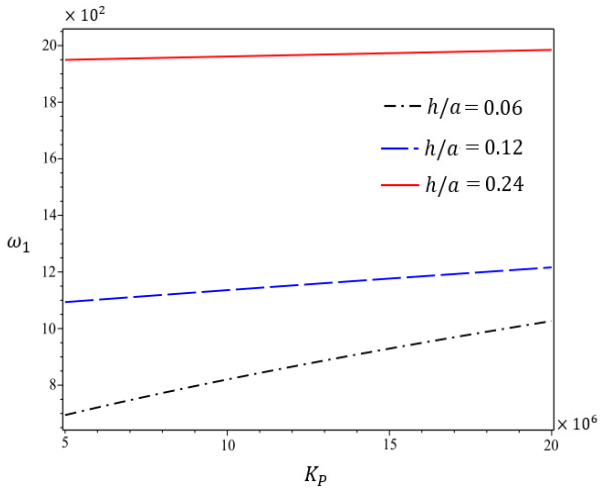

Figure 14. The first linear frequency variation with the shear layer stiffness change for different values of the thickness ratio.

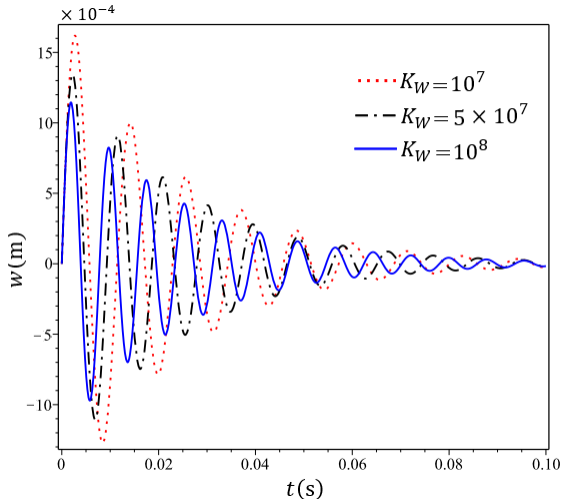

Figure 15. The deflection of the studied beam with the damping time change for different Winkler's spring modulus.

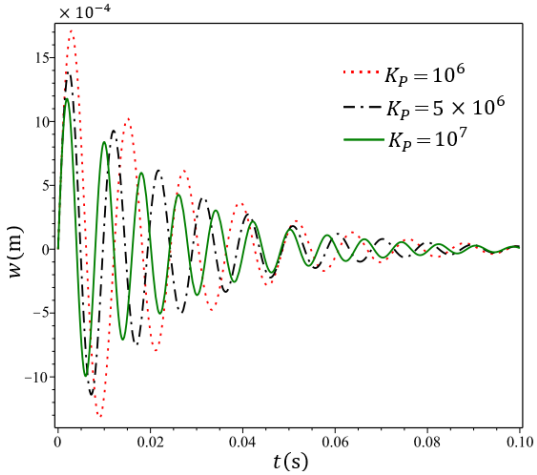

Figure 16. The deflection of the studied beam with the damping time change for different values of the shear foundation (Pasternak's) constant.

Variation of the closed-loop frequencies and damping coefficients concerning the changes in foundation parameters and the compression force (positive in-plane force) and extensional or tension force (negative in-plane force) is presented in Table 3 for two different positions of the active inner layers. Effect of the shear layer stiffness on the frequencies more than the influence of Winkler's spring modulus. It can be seen that there is no clear effect of the foundation constants on the damping coefficients, whereas the frequency values rise by increasing values of the foundation constants (K_W or K_P) as shown in Figure 8. Figures 9 and 10 illustrate that the first linear frequency variation with the feedback gain control change is very slight with the feedback gain control change for different values of the Winkler's spring modulus and the shear layer stiffness, respectively. For various values of a feedback gain control constant, Figure 11 also shows that the influence of the shear layer stiffness change on the first damping coefficient variation is very slight. For different values of Winkler's spring modulus and the shear layer stiffness, Figures 12 and 13 show the linear frequency increases highly with the half-wave number rise. The linear fundamental frequency variation with the shear layer stiffness change is displayed in Figure 14 for different values of the thickness ratio. It can be noted that the frequencies increase whenever the shear layer stiffness rises but this effect is clear for thin beams more than thick ones. Furthermore, the central displacement behavior of the proposed beam with the damping time variation is presented for various values of Winkler's spring modulus in Figure 15, and for various values of Pasternak's constant in Figure 16. The figures show that the deflection suppression process improves by increasing the Winkler's spring and shear layer stiffness where the system needs a shorter interval for control the deflection suppression time.

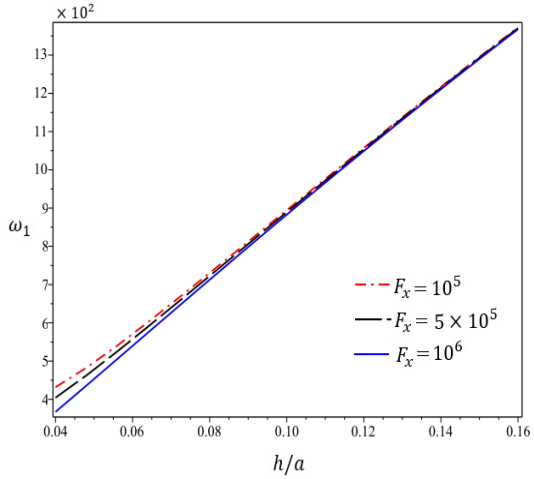

Figure 17. The first linear frequency variation with the thickness ratio change for different values of the compression force.

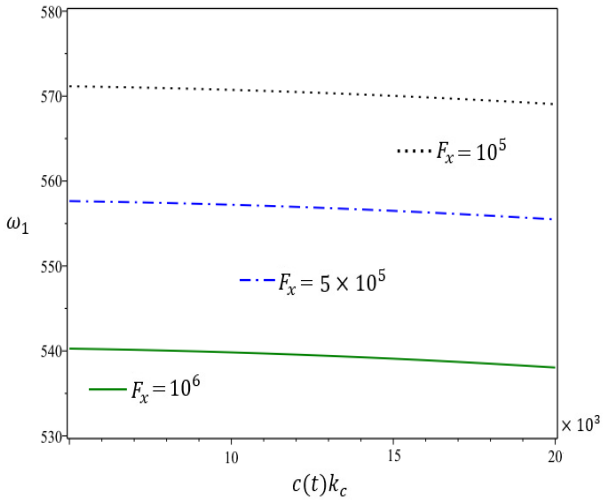

Figure 18. The first linear frequency variation with the feedback gain control change for different values of the compression force.

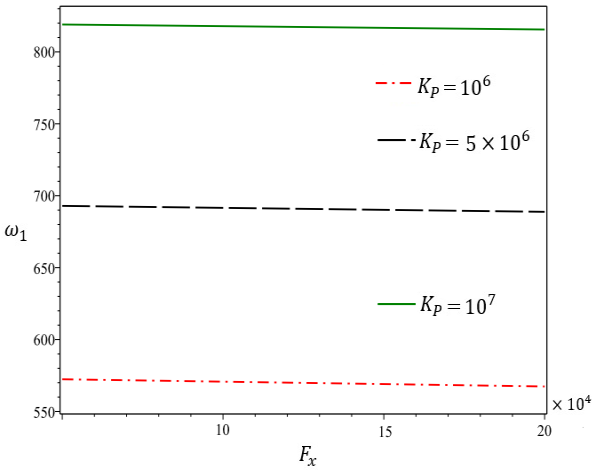

Figure 19. The first linear frequency variation with the compression force change for different values of the shear layer stiffness constant.

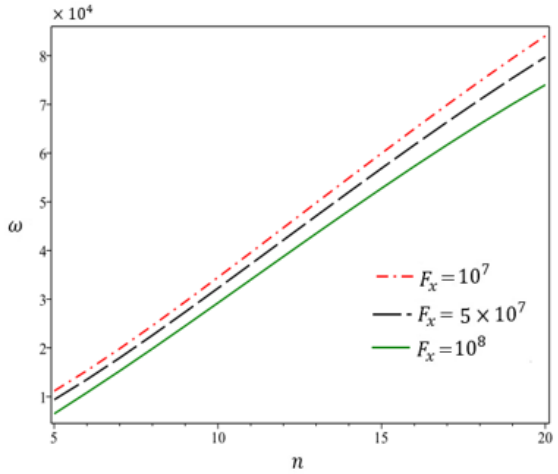

Figure 20. The linear frequency variation with the mode number change for different values of the compression force.

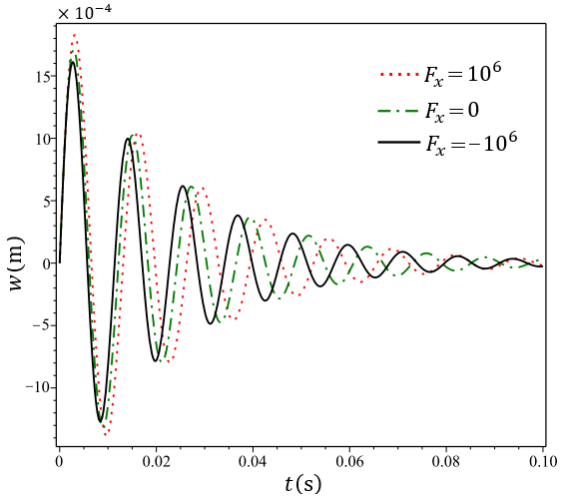

Figure 21. The deflection of the studied beam with the damping time change for different in-plane force values.

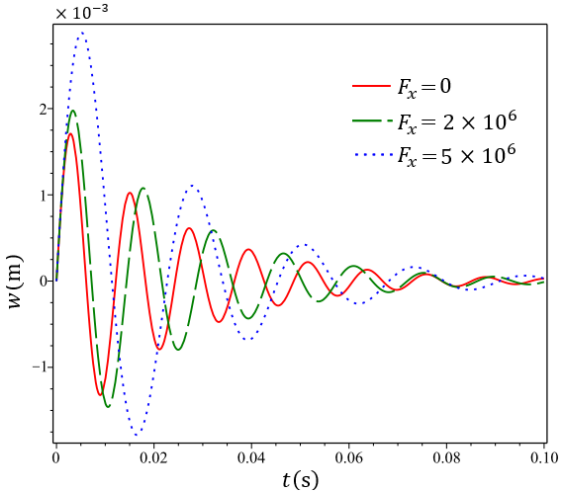

Figure 22. The deflection of the studied beam with the damping time change for different compression force values.

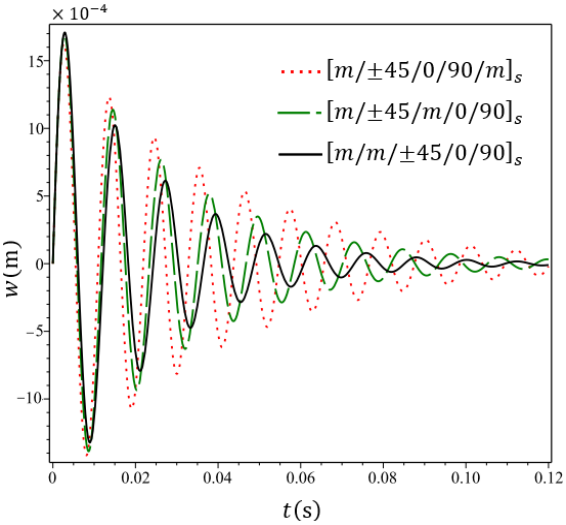

Figure 23. The deflection behavior of the studied beam with the damping time change for different positions of the inner magnetostrictive layers.

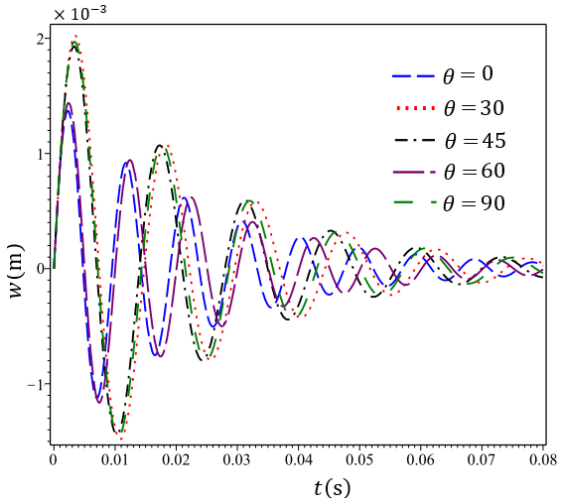

Figure 24. The central deflection of the beam with lamination scheme $[m/m/\theta/\theta/\theta/\theta]_s$ for various orientations of the layer's fiber.

The influence of the compression and tension forces on the closed-loop frequencies and damping coefficients also can be deduced from Table 3. It is observed that there is no effect of in-plane forces on the damping coefficients. Whereas the fundamental frequency increases by increasing the extensional force, and it decreases by increasing the compression force. The compression force effect on fundamental frequency is obvious for a thin beam more than a thick one as appeared in Figure 17. Figure 18 shows that the increasing of feedback gain control value leads to the force effect reduction on the system frequency slightly. The system frequency increases whenever the shear layer stiffness rises but this effect reduces slightly with the compression force increases as displayed in Figure 19. Moreover, the system frequency decreases whenever the compression force increases but this influence reduces with the mode number rises where the frequency increases obviously by increasing the modes as displayed in Figure 20.

Figures 21 and 22 present the effects of the compression and tension forces on the central deflection with the time change. The comparison between in-plane forces (the compression and extensional forces) on the system deflection is illustrated in Figure 21. It is noted that the compression force leads to the deflection increases, whereas, the deflection decreases due to the extensional force effect. Also, the deflection increases due to increasing the compression force value as a result of frequencies decrease as shown in Figure 22. Furthermore, it seems from the results in the tables that the location of the magnetostrictive actuating layers plays a vital role in vibration control of the studied system. Figure 23 shows the central deflection with the damping time variation for different positions of the internal magnetostrictive layers. The vibration suppression process improves as the internal actuators move away from a core of the plate and toward faces of the plate. Finally, influence of the layer's fiber orientations on the central deflection is presented in Figure 24 for the lamination scheme $[m/m/\theta_4]_s$. It can be noted that the $[m/m/0_4]$ has the highest flexural rigidity due to it presents the highest frequencies among the studied cases, whereas the $[m/m/30_4]$ represents the lowest flexural rigidity.

Conclusions

Using four Terfenol-D actuators and a simple feedback gain control system, control of dynamic response for laminated composite beam rested on Pasternak's foundation have been carried out

under the effect of an external force in x-direction and a magnetic field. Influence of the thickness ratio, ply orientations, location of magnetostrictive layers, foundation stiffness, velocity feedback gain value, and external force on the closed-form solution for dynamic characteristics of magnetostrictive/fiber-reinforced laminated composite sandwich beam has been investigated. The next outstanding results have been deduced:

- Increasing stiffness of the shear layer leads to the frequencies increase, and the time and deflection reduce.
- The eigenfrequencies and deflections are influenced by the thickness ratio and half-wave numbers significantly where increasing of these factors leads to vibration damping improvement.
- The layer's fiber orientations and position of the magnetostrictive layers play obvious roles in the vibration control process of the system.
- The suppression time is directly proportional to the positive in-plane force and inversely proportional to the negative in-plane force, whereas the inverse influence happens in the frequencies of the system.
- Hence, the stability of the smart laminated composite beam can be improved by selecting the optimum values of the control gain of the applied magnetic field, optimum layer's fiber orientations, and optimum position of the magnetostrictive layers.

References

[1] Tan X.B, Baras J.S., 2004, Modeling and control of hysteresis in magnetostrictive actuators, *Automatica* 40(9): 1469–1480.
[2] Z. Deng, M.J Dapino, 2018, Review of magnetostrictive materials for structural vibration control, *Smart Materials and Structures* 27: 113001.
[3] Amabili M., Farhadi S., 2009, Shear deformable versus classical theories for nonlinear vibrations of rectangular isotropic and laminated composite plates, *Journal of Sound and Vibration* 320: 649–667.
[4] Amabili M., 2008, Nonlinear Vibrations and Stability of Shells and Plates, *Cambridge University Press*, New York, USA.
[5] Nejad M.Z., Jabbari M., Hadi A., 2017, A review of functionally graded thick cylindrical and conical shells, *Journal of Computational Applied Mechanics* 48(2): 357–370.
[6] Murty A.V.K., Anjanappa M., Wu Y.F., 1997, The use of magnetostrictive particle actuators for vibration attenuation of flexible beams, *Journal of Sound and Vibration* 206(2): 133–149.
[7] Kumar J.S., Ganesan N., Swarnamani S., Padmanabhan C., 2003, Active control of beam with magnetostrictive layer, *Computers & Structures* 81(13): 1375–1382.
[8] Kumar J.S., Ganesan N., Swarnamani S., Padmanabhan C., 2003, Active control of cylindrical shell with magnetostrictive layer, *Journal of Sound and Vibration* 262(3): 577–589.
[9] Lee S.J., Reddy J.N., 2004, Rostam-Abadi F., Transient analysis of laminated composite plates with embedded smart-material layers, *Finite Elements in Analysis and Design* 40(5-6): 463–483.
[10] Pradhan S.C., 2005, Vibration suppression of FGM shells using embedded magnetostrictive layers, *International Journal of Solids and Structures* 42(9-10): 2465–2488.
[11] Zabihollah A., Zareie S., 2011, Optimal design of adaptive laminated beam using layerwise finite element, *Journal of Sensors* 2011: 240341.
[12] Reddy J.N., 1999, On laminated composite plates with integrated sensors and actuators, *Engineering Structures* 21: 568–593.
[13] Santapuri S., Scheidler J.J., Dapino M.J., 2015, Two-dimensional dynamic model for composite laminates with embedded magnetostrictive materials, *Composite Structures* 132: 737–745.
[14] Krishnamurthy A.V., Anjanappa M., Wang Z., Chen X., 1999, Sensing of delaminations in composite laminates using embedded magnetostrictive particle layers, *Journal of Intelligent Material Systems and Structures* 10(10): 825–835.
[15] Hong C.C., 2013, Application of a magnetostrictive actuator, *Mater. Des*., 46: 617–621.
[16] Moon S.J., Lim C.W., Kim B.H., Park Y., 2007, Structural vibration control using linear magnetostrictive actuators, *Journal of Sound and Vibration* 302(4–5): 875–891.

[17] Kishore M.D.V.H., Singh B.N., Pandit M.K., 2011, Nonlinear static analysis of smart laminated composite plate, *Aerospace Science and Technology* 15: 224–235.
[18] Zhou H-M., Zhou Y-H., 2007, Vibration suppression of laminated composite beams using actuators of giant magnetostrictive materials, *Smart materials and structures* 16(1): 198.
[19] Oates W.S., Smith R.C., 2008, Nonlinear optimal control techniques for vibration attenuation using magnetostrictive actuators, Journal of Intelligent *Material Systems and Structures* 19(2): 193–209.
[20] Xu X., Han Q., Chu F., 2017, Nonlinear vibration of a rotating cantilever beam in a surrounding magnetic field, International *Journal of Non-Linear Mechanics* 95: 59–72.
[21] Zhang Y., Zhou H., Zhou Y., 2015, Vibration suppression of cantilever laminated composite plate with nonlinear giant magnetostrictive material layers, *Acta Mechanica Solida Sinica* 28: 50–61.
[22] Zhou H.M., Zheng X.J., Zhou Y-H., 2006, Active vibration control of nonlinear giant magnetostrictive actuators, *Smart Materials and Structures* 15(3): 792.
[23] Shindo Y., Narita F., Mori K., Nakamura T., 2009, Nonlinear bending response of giant magnetostrictive laminated actuators in magnetic fields, *Journal of Mechanics of materials and structures* 4(5): 941–949.
[24] Saidha E., Naik G.N., Gopalkrishnan S., 2003, An experimental investigation of a smart laminated composite beam with a magnetostrictive patch for health monitoring applications, *Structural Health Monitoring* 2(4): 273–292.
[25] Zhang B., Jin K., Kou Y., Zheng X., The model of active vibration control based on giant magnetostrictive materials, *Smart Materials and Structures* 28(8): 085028, 2019.
[26] Shahin M., Asghar J.A., 2019, Vibration suppression of truncated conical shells embedded with magnetostrictive layers based on first order shear deformation theory, *Journal of Theoretical and Applied Mechanics* 57(4): 957–972.
[27] Zenkour A.M., El-Shahrany H.D., 2019, Vibration suppression analysis for laminated composite beams contain actuating magnetostrictive layers, *Journal of Computational Applied Mechanics* 50(1): 69–75.
[28] Zenkour A.M., El-Shahrany H.D., 2020, Vibration suppression of magnetostrictive laminated beams resting on viscoelastic foundation, *Applied Mathematics and Mechanics* 41: 1269–1286.
[29] Zenkour A.M., El-Shahrany H.D., 2021, Quasi-3D theory for the vibration and deflection of a magnetostrictive composite plate resting on a viscoelastic medium, *Composite Structures* 269: 114028.
[30] Reddy J.N., Barbosa J.I., On vibration suppression of magnetostrictive beams, *Smart Materials and Structures* 9: 49–58, 2000.
[31] Barati A., Adeli M.M., Hadi A., 2020, Static torsion of bi-directional functionally graded microtube based on the couple stress theory under magnetic field, *International Journal of Applied Mechanics*, doi.org/10.1142/S1758825120500210.
[32] Barati A., Hadi A., Nejad M.Z., Noroozi R., 2020, On vibration of bi-directional functionally graded nanobeams under magnetic field, Mechanics Based Design of Structures and Machines 1–18.
[33] Mousavi M., Hosseini M., Hadi A., Shishehsaz M., 2020, Bending Analysis of Bi-Directional FGM Timoshenko Nano-Beam subjected to mechanical and magnetic forces and resting on Winkler-Pasternak foundation, International Journal of Applied Mechanics, doi. 10.1142/S1758825120500933.